Computation of localized post buckling in long axially compressed cylindrical shells

G. J. Lord, A. R. Champneys and G. W. Hunt

Email alerting service	Receive free email alerts when new articles cite this article - sign up in the box at the top right-hand corner of the article or click **here**

Computation of localized post buckling in long axially compressed cylindrical shells

By G. J. Lord[1], A. R. Champneys[1] and G. W. Hunt[2]

[1]Department of Engineering Mathematics, University Walk,
University of Bristol, Bristol BS8 1TR, UK
[2]Department of Mechanical Engineering, University of Bath, Bath BA2 7AY, UK

Buckling is investigated of a long thin cylindrical shell under longitudinal compression as modelled by the von Kármán–Donnell equations. Evidence is reviewed for the buckling being localized to some portion of the axial length. In accordance with this observed behaviour the equations are first approximated circumferentially by a Galerkin procedure, whereupon cross-symmetric homoclinic solutions of the resulting system of ordinary differential equations are sought in the axial direction. Results are compared with experimental and other numerical data. Excellent agreement with experiments is achieved with fewer approximating modes than other methods.

1. Introduction

The buckling of a long thin circular cylindrical shell under axial compression is one of the classic problems of structural mechanics. If overall (strut or Euler) buckling is suppressed, experiments under rigid loading indicate a highly unstable snapback response, as described, for example, in Donnell (1934) or Yamaki (1984), in which a finite-amplitude buckle pattern appears instantaneously, accompanied by a dramatic drop in load (see figure 1). In addition, the system is notoriously imperfection sensitive (Koiter 1945). To quote Donnell & Wan (1950), referring to a particular set of experiments:

> Buckling comes suddenly, almost explosively, and usually occurs over only part of the wall.... The number of waves around the circumference is of the order of ten or so, and the wave shape ratio (ratio of wavelength in the circumferential to that in the axial direction) is always close to unity, with an average value of about 0.75.

This suggests that, while periodicity governs circumferentially, axially the buckle pattern may localize. A standard analytical approach adopted by Koiter (1945) and others is to assume that this pattern comprises a complex interaction of a number of linear *modes*, associated with zero eigenvalues at the critical load of the perfect system, that are periodic both axially and circumferentially. The governing equations do indeed admit such solutions, but it has emerged recently via double-scale asymptotic analysis that axially localized solutions are also admissible (Hunt & Lucena Neto 1991, 1993). Such behaviour has only been validated close to the theoretical critical load, yet real (imperfect) shells buckle at some fraction, perhaps 25%, of that load. This thoroughly unstable post-buckling characteristic led in the 1960s to

a search for the so-called *minimum post-buckling load* that can be sustained in the buckled regime, a quest effectively ended by Hoff *et al.* (1966), who demonstrated for outright periodicity that it tends to fall to zero as shell thickness approaches zero. This would be expected from the periodic form of the *Yoshimura* or *diamond* pattern (Yoshimura 1930), that can be folded out of a flat sheet of paper and thus exist at zero load without membrane stretching.

For responses that localize axially, none of these arguments need apply. The need for non-zero membrane strain energy in a *localized* Yoshimura state means that some external loading is required, and the minimum localized post-bucking load is thus greater than zero. Hunt & Lucena Neto (1993) suggest, purely on asymptotic grounds, that the Maxwell critical load for periodic buckling (when energy levels are the same in the fundamental and restabilized post-buckled states) might represent a good approximation to the minimum post-buckling load for an associated localized response. Experimental correlation based on a small sample set (Yamaki 1984) is good, but until now numerical confirmation away from the asymptotic limit has been lacking.

The most widely used model for the buckling of thin cylinders rests with the von Kármán–Donnell equations, a coupled pair of nonlinear fourth-order partial differential equations (PDEs) governing radial displacement, w, and in-plane stress function, ϕ. We consider an infinitely long cylinder and discretize the von Kármán–Donnell equations circumferentially by the Galerkin spectral method. This yields a system of ordinary differential equations (ODEs) in the axial variable x, for which we seek homoclinic (axially localized) solutions, with the axial length taken to be infinite. We claim that this infinite-length approximation is valid when one seeks localized solutions. This is confirmed below by the agreement found with experimental results on only moderately long cylinders.

The key idea behind the direct numerical methods for computing homoclinic orbits to equilibria is to pose the homoclinic orbit as a boundary value problem and then use the linearization about the fundamental state to define boundary conditions with the correct asymptotic behaviour on a truncated interval (Beyn 1990; Friedman & Doedel 1994). The technique of reducing to a set of ODEs to find localized solutions in elliptic equations has used by other authors, such as Mielke (1991), Hagstrom & Keller (1987) and Kirchgässner (1982).

Here the approach is adapted to a Galerkin approximation of the von Kármán–Donnell equations which retains circumferential periodicity. We seek solutions axially that are *cross-symmetric* (symmetric in even-numbered waves and anti-symmetric in odd-numbered waves) about a section through the cylinder, as observed experimentally (Yamaki 1984); results on symmetric and other possible forms will be presented elsewhere. Buckling paths are investigated as the load parameter is varied by numerical continuation using the code AUTO (Doedel & Kernevez 1986). A detailed presentation of the numerical homotopies required to obtain an initial solution at fixed load is deferred to later work.

The remainder of the paper is outlined as follows. Section 2 introduces the von Kármán–Donnell equations and their approximation: properties of low-order approximations are examined, and their numerical computation and suitability discussed. In § 3 we present numerical results for approximations of increasing order. Section 4 discusses the relevance of these results in the context of other work on cylinder buckling, and draws some general conclusions.

2. The von Kármán–Donnell equations and their approximation

Consider an infinitely long cylinder of radius R and shell thickness t. The classical equilibrium equations for the in-plane stress function ϕ and outward radial displacement displacement w in the post-buckling regime of the cylinder are given by the von Kármán–Donnell equations:

$$\kappa^2 \nabla^4 w + \lambda w_{xx} - \rho \phi_{xx} = w_{xx}\phi_{yy} + w_{yy}\phi_{xx} - 2w_{xy}\phi_{xy}, \tag{2.1}$$

$$\nabla^4 \phi + \rho w_{xx} = (w_{xy})^2 - w_{xx}w_{yy}, \tag{2.2}$$

where ∇^4 denotes the two dimensional biharmonic operator, $x \in \mathbb{R}$ is the axial and $y \in [0, 2\pi R]$ is the circumferential coordinate. The parameters appearing in (2.1) and (2.2) are the curvature $\rho := 1/R$,

$$\kappa^2 := t^2/12(1 - \nu^2),$$

where ν is Poisson's ratio and the bifurcation parameter

$$\lambda := P/Et,$$

where P is the compressive axial load applied per unit length and E is Young's modulus. Equations (2.1) and (2.2) are supplemented with periodic boundary conditions in y and asymptotic boundary conditions in the axial direction x: that w, ϕ and their x derivatives tend to zero (the fundamental solution) as $x \to \pm\infty$.

A standard periodic analysis of the von Kármán–Donnell equations is to seek the minimum load and corresponding axial and circumferential wavelengths such that a bifurcation occurs. Waves for which this is satisfied appear on the Koiter circle (Koiter 1945). For a discussion of mode interaction on the Koiter circle for the von Kármán–Donnell equations see Hunt & Lucena Neto (1991).

As stated in the introduction we perform a Galerkin approximation in the circumferential direction. We seek even periodic solutions to the von Kármán–Donnell equations in the circumferential direction y and hence use the cosine functions $\cos(m\rho y)$, $m \in \mathbb{N} \cup \{0\}$ as the basis functions in the Galerkin approximation.

The system (2.1) and (2.2) has a rich structure of symmetries (see Golubitsky *et al.* 1984; Hunt 1986; Hunt *et al.* 1986; Wohlever & Healey 1995). In order to examine deformations of the cylinder that remain within the subspace corresponding to invariance under rotation through $2\pi/s$, we introduce a seed mode $\psi_1^s = \cos(s\rho y)$ and let

$$w(y) = \sum_{m=0}^{\infty} a_m \psi_m^s, \quad \phi(y) = \sum_{m=0}^{\infty} b_m \psi_m^s,$$

where

$$\psi_m^s = \cos(ms\rho y), \quad m \in \mathbb{N} \cup \{0\}, \quad s \in \mathbb{N}.$$

Substituting into the von Kármán–Donnell equations, taking the L^2 innerproduct and expanding the nonlinear terms we find the following system of ODEs:

$$\kappa^2 \left\{ \frac{\partial^4 a_m}{\partial x^4} - 2s^2\rho^2 m^2 \frac{\partial^2 a_m}{\partial x^2} + s^4\rho^4 m^4 a_m \right\} + \lambda \frac{\partial^2 a_m}{\partial x^2} - \rho \frac{\partial^2 b_m}{\partial x^2}$$

$$= s^2\rho^2\chi \left\{ -\frac{1}{2} \sum_{k,\ell,m}^{\sim} \left(\ell^2 \frac{\partial^2 a_k}{\partial x^2} b_\ell + k^2 a_k \frac{\partial^2 b_\ell}{\partial x^2} \right) - \sum_{k,\ell,m}^{'} k\ell \frac{\partial a_k}{\partial x}\frac{\partial b_\ell}{\partial x} + \sum_{k,\ell,m}^{''} k\ell \frac{\partial a_k}{\partial x}\frac{\partial b_\ell}{\partial x} \right\},$$

$$\tag{2.3}$$

2140 *G. J. Lord, A. R. Champneys and G. W. Hunt*

$$\frac{\partial^4 b_m}{\partial x^4} - 2s^2 \rho^2 m^2 \frac{\partial^2 b_m}{\partial x^2} + s^4 \rho^4 m^4 b_m + \rho \frac{\partial^2 a_m}{\partial x^2}$$

$$= s^2 \rho^2 \tfrac{1}{2} \chi \left\{ \sum_{k,\ell,m}^{\sim} \ell^2 \frac{\partial^2 a_k}{\partial x^2} a_\ell + \sum_{k,\ell,m}^{'} k\ell \frac{\partial a_k}{\partial x} \frac{\partial a_\ell}{\partial x} - \sum_{k,\ell,m}^{''} k\ell \frac{\partial a_k}{\partial x} \frac{\partial a_\ell}{\partial x} \right\}, \quad (2.4)$$

for $m = 0, 1, 2, \ldots, \infty$, and where

$$\chi = \begin{cases} \tfrac{1}{2}, & m = 0, \\ 1, & \text{otherwise.} \end{cases}$$

The summations terms in (2.3) and (2.4) are defined for a given value of m by:

$$\sum_{k,\ell,m}^{\sim} := \sum_{\substack{k+\ell-m=0,\ k-\ell+m=0 \\ k-\ell-m=0,\ k,\ell \in \mathbb{N}\cup 0}}, \quad \sum_{k,\ell,m}^{'} := \sum_{\substack{k-\ell+m=0,\ k-\ell-m=0 \\ k,\ell \in \mathbb{N}\cup 0}}, \quad \sum_{k,\ell,m}^{''} := \sum_{\substack{k+\ell-m=0 \\ k,\ell \in \mathbb{N}\cup 0}}.$$

The Galerkin approximation is formed by taking equations (2.3) and (2.4) for $m = 0, \ldots, M-1$ only, for some finite M. Taking $s = 1$ corresponds to a standard Galerkin approximation discussed, for example, in Gottlieb & Orszag (1977), whereas $s > 1$ corresponds to seeking a solution in a specific subspace corresponding to the circumferential wave number s.

Note that there is a 'degeneracy' in the equations for the zero mode ($m = 0$) such that these could be solved with initial conditions for

$$\frac{\partial^2 a_0}{\partial x^2}, \frac{\partial^3 a_0}{\partial x^3}, \frac{\partial^2 b_0}{\partial x^2}, \frac{\partial^3 b_0}{\partial x^3},$$

independently of the initial conditions for a_0, b_0 and the first derivatives. This corresponds to a trivial translational symmetry in the problem.

The single mode approximation found by taking $M = 1$ ($m = 0$) in (2.3) and (2.4) yields a linear system for which there are no homoclinic solutions. Thus the simplest approximation for which we may expect to find a homoclinic orbit is the two mode approximation found by taking $M = 2$ ($m = 0, 1$) in (2.3) and (2.4). We truncate the system of ODEs (2.3) and (2.4) to a large finite interval, $x \in [0, T]$ and solve as a boundary value problem over half the length of the cylinder.

Boundary conditions are chosen at $x = 0$ to project out a linear approximation to the stable manifold of $a_k = b_k = 0$. This imposes the condition that the solution would leave the zero state along an unstable direction, as appropriate for the infinite length case (see, for example, Beyn 1990).

At $x = T$ we impose appropriate boundary conditions on the Fourier modes for solving over half the length of the cylinder. A number of choices, for example those exhibiting complete axial symmetry, are available. Here we attempt to match experiments by seeking solutions that we call (axially) *cross-symmetric*. These are solutions $w(x, y), \phi(x, y)$ which are invariant under the simultaneous application of $x \to 2T - x$ and $y \to y + \pi R/s$, but are in fact produced by symmetric conditions for the even-numbered modes and anti-symmetric conditions for the odd-numbered modes. An example of a cross-symmetric solution may be seen in the contour plot of figure 5. In contrast we refer to (axially) *symmetric* solutions as solutions which are symmetric in y about $x = T$ (i.e. $w(x, y)$ and $\phi(x, y)$ are invariant under $x \to 2T - x$ and $y \to y$).

In the parameter regime of interest the linearization of (2.3), (2.4) about the trivial solution yields four zero eigenvalues, $(4M - 2)$ eigenvalues in the left half plane and

$(4M - 2)$ eigenvalues in the right half plane. The non–zero eigenvalues occur in complex conjugate pairs. We see from the linearization that the equilibrium is not hyperbolic and instead has a centre-stable and centre-unstable manifolds. However, by inspection it is clear that these, the zero eigenvalues, and associated directions are a consequence of the 'degeneracy' in the zero mode. Thus, although we solve for the full system we consider the reduced linear problem for computing the projection boundary conditions at $x = 0$. The degeneracy in the zero mode forces the boundary conditions for that mode to be modified. The boundary value problem we solve is as follows. Rescale (2.3), (2.4) to the interval $[0, 1]$ and solve subject to the following.

(i) Boundary conditions at $x = 0$ for the zero mode ($m = 0$)

$$a_0(0) = 0, \quad \frac{\partial a_0(0)}{\partial x} = 0, \quad b_0(0) = 0, \quad \frac{\partial b_0(0)}{\partial x} = 0. \tag{2.5}$$

These four conditions impose that the solution is homoclinic to the flat equilibrium state, rather than some translate of it.

(ii) Standard projection boundary conditions for the non-zero modes ($m > 0$) at $x = 0$:

$$L_s(U(0) - 0) = 0, \tag{2.6}$$

where

$$U(0) := \left[a_1(0), \ldots, \frac{\partial^3 a_1(0)}{\partial x^3}, \ldots, a_{M-1}(0), \ldots, \frac{\partial^3 a_{M-1}(0)}{\partial x^3}, \right.$$

$$\left. b_1(0), \ldots, \frac{\partial^3 b_1(0)}{\partial x^3}, \ldots, b_{M-1}(0), \ldots, \frac{\partial^3 b_{M-1}(0)}{\partial x^3} \right]^{\mathrm{T}}$$

and L_s is the matrix whose rows span the left eigenspace of the corresponding stable (s) eigenvalues. This gives $4M - 2$ conditions.

(iii) Cross-symmetric section boundary conditions at $x = 1$ given by

$$\frac{\partial^2 a_0(1)}{\partial x^2} = 0, \quad \frac{\partial^2 b_0(1)}{\partial x^2} = 0, \tag{2.7}$$

$$\frac{\partial^i a_m(1)}{\partial x^i} = 0, \quad \frac{\partial^{i+2} a_m(1)}{\partial x^{i+2}} = 0, \quad \frac{\partial^i a_m(1)}{\partial x^i} = 0, \quad \frac{\partial^{i+2} b_m(1)}{\partial x^{i+2}} = 0, \tag{2.8}$$

for $m = 1, \ldots, M - 1$ and $i = 0$ if m is even and $i = 1$ if m is odd. These give a further $4M - 2$ boundary conditions.

In total we have $8M$ boundary conditions for $8M$ equations, which is the appropriate number for a well-posed problem. This boundary value problem can be solved by a regular continuation code, such as AUTO (Doedel & Kernevez 1986), to compute load–deflection bifurcation diagrams as in figure 2.

Initial approximations for the boundary value problems are found using a mixture of shooting and homotopy techniques. The details of the boundary conditions and the numerical techniques used for initial approximations will be discussed in later work where symmetric and other forms of solution will be considered.

3. Numerical Results

To compare with the experiments of Yamaki (1984) and the asymptotic analysis of Hunt & Lucena Neto (1993) calculations were performed for a shell with

$$\rho = 0.01 \, \mathrm{mm}^{-1}, \quad t = 0.247 \, \mathrm{mm}, \quad \nu = 0.3, \quad E = 5.56 \, \mathrm{GPa}.$$
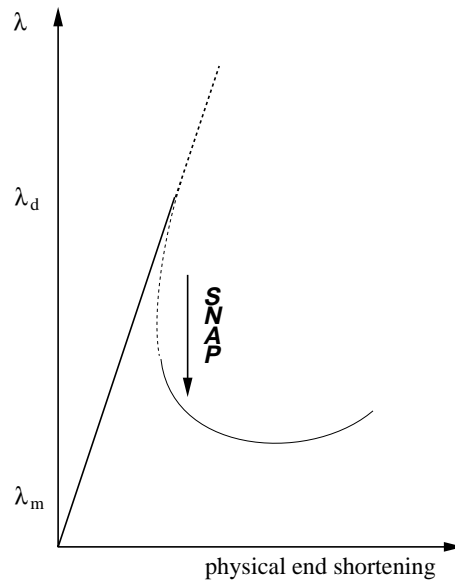
Figure 1. Schematic representation of expected response. The straight line represents the unbuckled state and the curved line the buckled state. Solid lines are stable, and dashed lines unstable, equilibrium states under rigid loading conditions.

Yamaki's experiments were carried out for clamped cylindrical shells —we consider here results from the longest of such shells, length $L = 160.9$ mm. Note that even this could hardly be described as long, since its aspect ratio (length to diameter) is only $L/2R \approx 0.8$. Yamaki found buckle patterns which were both symmetric and cross-symmetric; the solutions presented here will all be cross-symmetric.

We compare with experiments the minimum ($W_{\min}$) and maximum ($W_{\max}$) values of the displacement w, and the ratios

$$\lambda_{\mathrm{m}}/\lambda_{\mathrm{d}}, \quad \beta = \frac{\text{axial wavelength at } \lambda_{\mathrm{m}}}{\text{circumferential wavelength at } \lambda_{\mathrm{m}}},$$

where λ_{d} denotes the smallest value of λ at which the fundamental solution bifurcates, and λ_{m} corresponds to the minimum post buckling load. For the Yamaki cylinder described above it is easily shown that $\lambda_{\mathrm{d}} \approx 1.494912 \times 10^{-3}$. For the numerical simulations, λ_{m} was taken to be the first limit point on the branch of homoclinics as the load was decreased (corresponding to the minimum of the curves in figure 2). For the *aspect ratio*, β, only the axial wavelength was required from the simulations, since the circumferential wave number and hence corresponding wavelength were known. The axial wavelength was defined to be twice the axial distance between a maximum and a minimum, that is twice the distance between the point P and Q on the contour plot (figure 5). This quantity was estimated from the line $y = 0$.

In the bifurcation diagram (figure 2), we plot the loading parameter, λ, against a measure of the end shortening defined by

$$\int_{-\infty}^{\infty} |w_x(x, y)| \, \mathrm{d}x = \int_{-\infty}^{\infty} \left| \sum_{k=0}^{\infty} \frac{\partial}{\partial x} (a_k(x) \cos(ks\rho y)) \right| \mathrm{d}x,$$

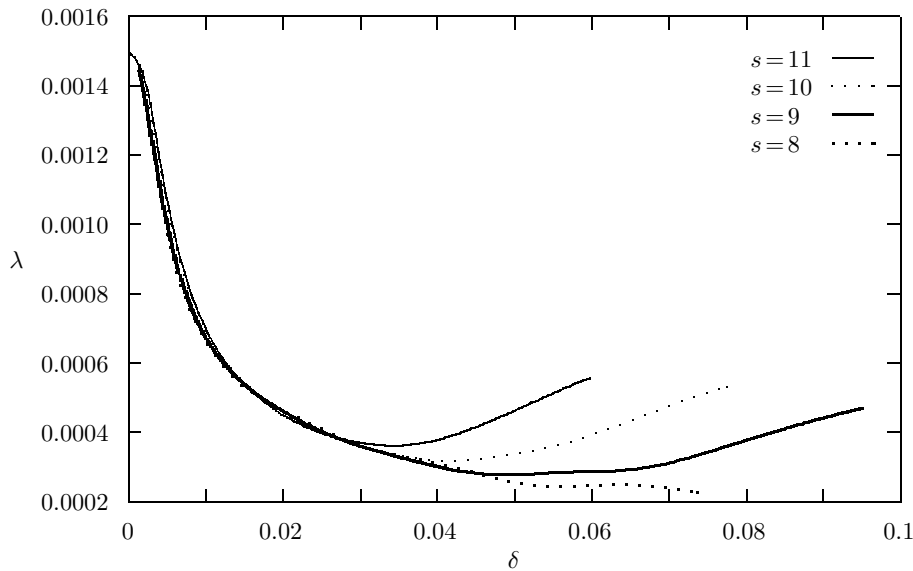which in general varies with y. For simplicity we take $y = 0$ and measure over the

Figure 2. Bifurcation diagram showing the load parameter λ against a measure of end-shortening δ for wave numbers $s = 8$, 9, 10 and 11.

Table 1. *Convergence of the minimum load* λ_{m}, *ratio of wavelengths* β *and the minimum and maximum displacements* $W_{\min}$ *and* $W_{\max}$ *as the number of modes in the approximation is increased*

$s = 11$	$M = 2$	$M = 3$	$M = 4$	$M = 5$	$M = 6$
$\lambda_{\mathrm{m}}/\lambda_{\mathrm{d}}$	0.1515	0.1938	0.2321	0.2436	0.2418
β	2.123	1.819	1.571	1.789	1.741
$W_{\min}$	-0.742	-0.946	-1.018	-0.839	-0.866
$W_{\max}$	1.622	1.959	2.192	1.919	1.966

half length of the cylinder to get,

$$\delta = \int_0^{\mathrm{T}} \left| \sum_{k=0}^{M-1} \frac{\partial a_k}{\partial x} \right| \mathrm{d}x. \tag{3.1}$$

We use this as a *measure* of the end-shortening, but note that it bears no direct relation to *actual* end shortening of a specimen cylinder: more physically meaningful measures will be considered in future work. As the pure-squash component of δ is absent from the present formulation, the 'snapback' phenomenon indicated in the schematic diagram of figure 1 is only implied in the plotted bifurcation diagram of figure 2. The λ axis of figure 2 thus corresponds to the sloped line in the schematic figure 1. Note that in practice one would only expect to see the stable portions of the curves, as for example in Yamaki's experiments.

We note that in the computations below the half length of the cylinder T was either taken to be $T = 300$ or, for direct comparison with Yamaki, $T = 100$. The values for λ_{m}, $W_{\min}$, $W_{\max}$ and β were found to be essentially independent of the length of the interval T solved over in accordance with results of Beyn (1990), Schecter (1993) and
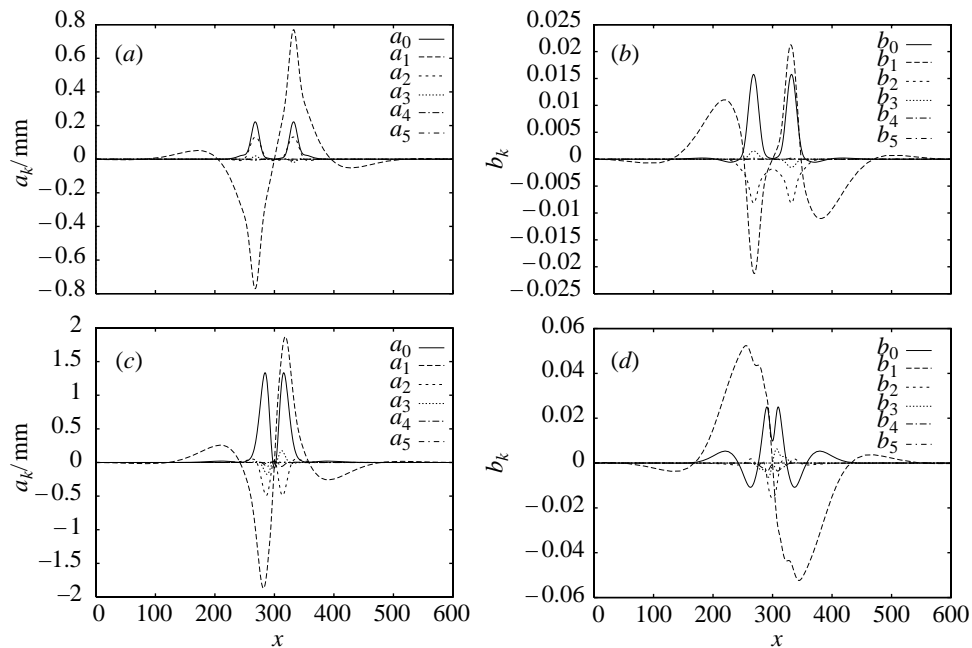
Figure 3. Fourier modes a_k and b_k for the displacement, w, and stress function, ϕ, respectively, at $\lambda = 5 \times 10^{-4}$. ($a$), ($b$) As the load is decreased from λ_d before the minimum load λ_m and (c), (d) after the minimum load λ_m.

Sandstede (1996). In the figures that follow, x is plotted on $[0, 2T]$, y is plotted on $[0, 2\pi R]$ and x, y, W_min, W_max and the Fourier coefficients a_k are measured in mm.

(a) *Results*

We compare our results to the cross-symmetric results of Yamaki (1984). For the shell under consideration Yamaki describes in some detail the case of 11 circumferential waves ($s = 11$) close to the minimum load λ_m. The case $s = 11$ was also considered by Hunt & Lucena Neto (1993); although dependent on R/t, this is typical of the number of circumferential modes observed experimentally (recall the quote from Donnell & Wan (1950) in the introduction). We present results for $s = 8$, 9, 10 and 11 and consider in greater detail the case $s = 11$.

First we examine convergence of the numerics as the number of circumferential modes used in the approximation is increased. The computations were performed for wave number $s = 11$. In table 1 we present values of $\lambda_\mathrm{m}/\lambda_\mathrm{d}$, β, and minimum and maximum values of the displacement, W_min and W_max, as M is increased to a maximum of six. We see that $M = 6$ appears to give convergence to one decimal place in all four quantities. All further results presented were computed with $M = 6$.

In figure 2 we have plotted the bifurcation diagram of load, λ, versus end shortening, δ, for $s = 8$, 9, 10 and 11. Note from the diagram that as the circumferential wave number decreases, the minimum load λ_m decreases and the end shortening at this minimum load increases. This corresponds with experimental evidence depicted in figure 3.52e (a) of Yamaki (1984). Unlike the experimental solutions, our numerical solutions do not 'feel' their stability, and hence we are able to compute the bifurcation curves back to the originating bifurcation point λ_d.

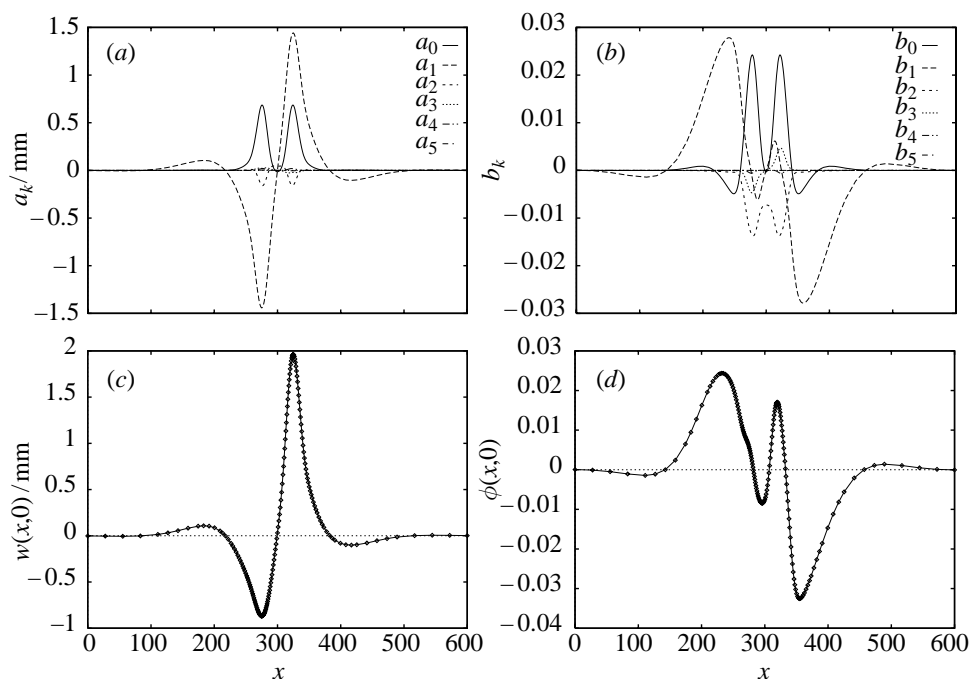We next present detailed results for wave number $s = 11$. Figure 3 shows the

Figure 4. At the minimum load λ_m. (*a*) Fourier modes a_k for displacement w; (*b*) Fourier modes b_k for the stress function ϕ; (*c*) Reconstructed solution $w(x,0)$; and (*d*) $\phi(x,0)$.

Fourier modes a_k, b_k, ($k = 0, 1, 2, 3, 4, 5$) for the displacement w and stress function ϕ, respectively, before and after the minimum load λ_m. In (*a*) and (*b*) a_k and b_k are plotted at $\lambda = 5 \times 10^{-4}$ before the minimum load λ_m is reached (decreasing λ from λ_d) and in (*c*) and (*d*) a_k and b_k are re-plotted at the same value of λ but after passing through λ_m. Note that the solutions appear quite different. Comparing (*a*) to (*c*) and (*b*) to (*d*) shows that the magnitude of both the Fourier modes a_k and b_k is larger having passed through λ_m and that the Fourier modes appear more localized.

Figure 4 depicts the solution when the load λ is at the minimum load λ_m. In figure 4a we have plotted the Fourier modes a_k for the displacement w and in (*b*) the modes b_k for the stress function ϕ. In figure 4c we have reconstructed the solution $w(x,y)$ at $y = 0$ and in (*d*) we have plotted the $\phi(x,y)$ at $y = 0$.

Figure 5 shows the contour map of the displacement, w, plotted over the cylinder at the minimum load λ_m, with the values of certain contours marked. The cross-symmetric nature of the solution over the whole cylinder is clearly evident from this plot. The circumferential wave number, s, is easily verified as 11 and we have indicated on the diagram half the axial wavelength—the distance between P and Q. The reader may wish to compare this plot to the contour plots in Yamaki (1984, figure 3.52e (*b*)).

In figure 6 we have reconstructed the full solution $w(x,y)$ and in figure 7 we have reconstructed the full solution $\phi(w,y)$ at the minimum load λ_m for $s = 11$. In each case contours are plotted over the deformed cylinder, with the colour bar indicating the magnitude of w or ϕ. Note that the length of the cylinder is 200 mm which is comparable to the length of the Yamaki cylinder.

We now consider the *quantitative* agreement with the experiments. Table 2 presents a full comparison with the experimental and fully periodic numerical results of Yama-
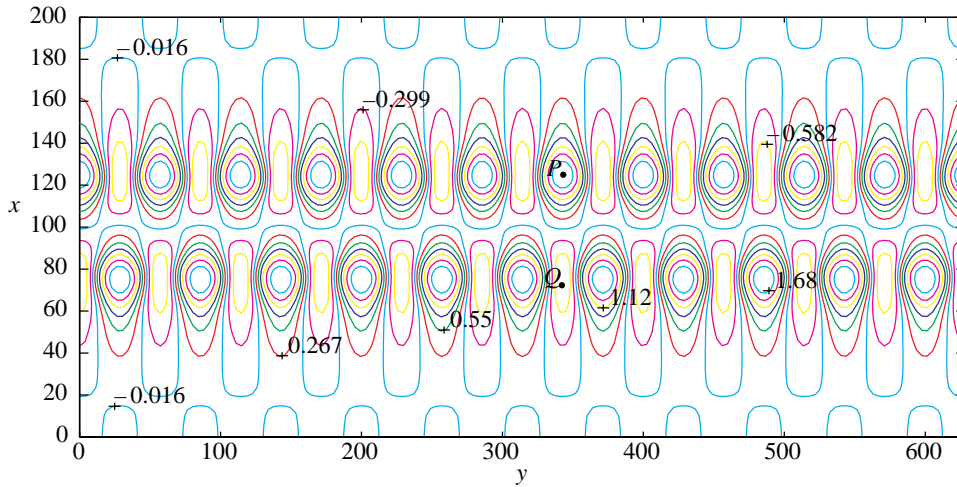
Figure 5. Contour plot for the cross-symmetric form of solution of the outward buckling displacement, w, at the minimum value of the buckling load parameter $\lambda = \lambda_m$. $x \in [0, 2T]$ is the axial coordinate and $y \in [0, 2\pi R]$ is the circumferential coordinate. Also indicated is half axial wavelength (PQ): details in text.
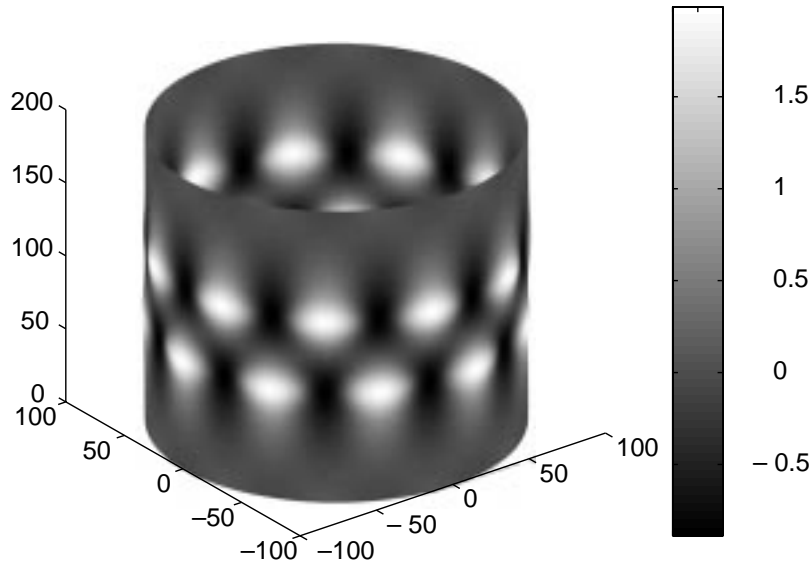

Figure 6. Reconstructed displacement $w(x, y)$ plotted over the deformed cylinder for $s = 11$.

ki (1984), and with the asymptotic results of Hunt & Lucena Neto (1993) based upon the Maxwell concept. For the seed modes $s = 10$ and $s = 11$ we see good agreement in the minimum load λ_m and also in the minimum and maximum displacements $W_{\min}$ and $W_{\max}$. However, as the wave number is decreased our results and those of Hunt & Lucena Neto (1993) tend to drift from the experimental values; there are also growing differences in the aspect ratio, β. For $s = 9$ and $s = 8$, the results indicate that the six modes a_0 to a_5 may not be enough for convergence. Boundary conditions would also be expected to have a greater part to play for the longer wavelength modes.
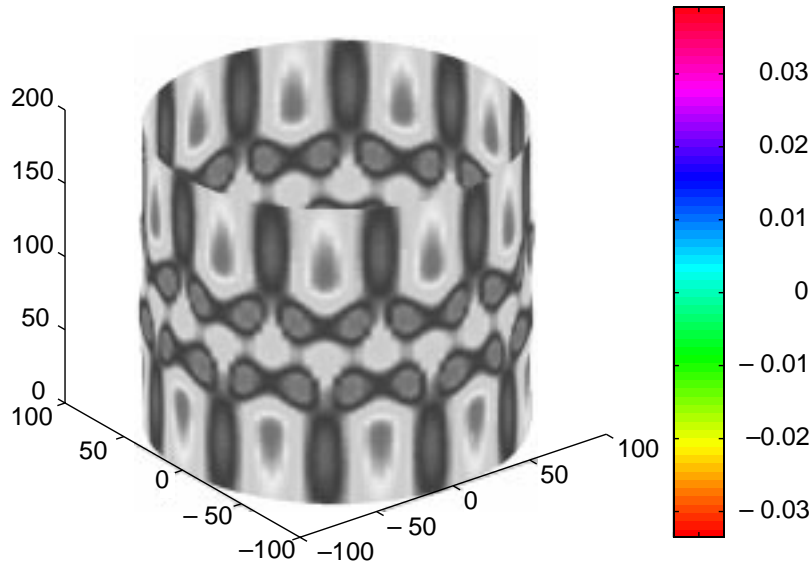
Figure 7. Reconstructed stress function $\phi(x, y)$ plotted over the deformed cylinder for $s = 11$.

Table 2. *Comparison of results*

	s	present $M = 6$	(Yamaki 1984) experimental	periodic	(Hunt & Lucena Neto 1993) asymptotics
$\lambda_{\mathrm{m}}/\lambda_{\mathrm{d}}$	11	0.242	0.24	0.26	0.24
	10	0.213	0.21	0.22	0.21
	9	0.185	0.17	0.17	0.18
	8	0.163	0.14	0.12	0.16
β	11	1.74	1.43[a]	1.54[a]	1.49
	10	1.84			1.51
	9	1.96			1.56
	8	2.13	1.37[a]	1.42[a]	1.60
$W_{\min}$	11	−0.866	−0.9	−0.89	−1.09
	10	−1.075	−1.0	−1.24	−1.36
	9	−1.411	−1.56	−1.56	−1.68
	8	−1.894	−1.9	−1.90	−2.15
$W_{\max}$	11	1.966	1.9	1.90	2.47
	10	2.384	2.6	2.52	3.01
	9	2.852	3.2	3.21	3.73
	8	3.291	4.0	4.03	4.77

[a] Indicates that this was not at a minimum load.

A plausible explanation for why the wavelengths we observe numerically do not match those of experiments is that there is a large sensitivity of β to the value of λ near λ_{m} and that the experimental wavelengths given in the table are taken for values of the load λ close to, but not exactly at, the minimum load λ_{m} (compare figure 3.52e (*b*) and table 3.7 pages 231 and 232 in Yamaki (1984)). This sensitivity can be verified from our numerics. Figure 8 shows the load, λ, plotted against the
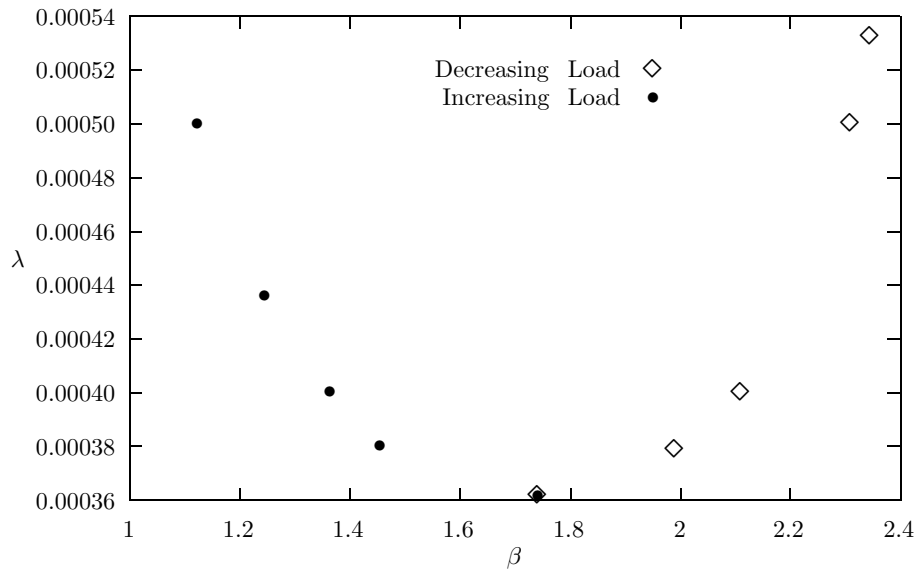
Figure 8. Plot of β as the load is decreased ($\diamond$) to the minimum value λ_{m} and is increased ($\bullet$) past λ_{m}.

buckle pattern aspect ratio, β, for $s = 11$ with $M = 6$. As λ is decreased from the bifurcation value λ_{d} we see that β also decreases. As λ continues through the limit point and starts to increase, β continues to decrease. What is clear is that close to the limit point a small variation in λ leads to a large variation in β. Indeed the curve appears to be well fitted (in the least squares sense) close to the minimum λ_{m} by a quartic

$$\lambda_p(\beta) = 0.0006\beta^4 - 0.004\beta^3 + 0.01\beta^2 - 0.0121\beta + 0.0058, \tag{3.2}$$

in which case the points λ (shown in figure 8) are given by $\lambda = \lambda_p + \epsilon$ where the error ϵ has a maximum value of $\epsilon = 3.053 \times 10^{-6}$. Furthermore we can test this against the experiments: Yamaki (1984) found that $\beta = 1.43$, which from (3.2) suggests that a load of $\lambda \approx 3.8501 \times 10^{-4}$; in fact the experimental value was $\lambda = 3.743 \times 10^{-4}$. The fast variation of the axial wavelength around the minimum value indicates that there is a large scope for error in estimating this particular parameter and that the data for the Yamaki cylinder is for a value of λ just past the minimum load λ_{m}.

4. Discussion and conclusion

This paper demonstrates excellent qualitative and quantitative agreement between numerics and experiments. The agreement is particularly good considering our analysis is for an infinitely long cylinder, whereas the comparison is with a moderately long cylinder of aspect ratio (length to diameter) of approximately 0.8. Results are essentially independent of chosen (structural) boundary conditions, the only criterion being that at the boundaries the solution lies either on the stable, or the unstable, manifold. The experimental displacements and the minimum load values are well matched by the numerics. We have shown that the axial wavelength measured by β varies rapidly with λ around the minimum load λ_{m}, this sensitivity explaining the discrepancy in the values of β.

Particularly good agreement is found for circumferential wave numbers $s = 10$ and

$s = 11$; however, for $s = 8$ and $s = 9$ a slight discrepancy between the numerical and experimental values is observed. Preliminary evidence suggests that, although convergence is achieved for $s = 11$, more modes are required to fully resolve the solution for $s \leqslant 9$. Indeed Yamaki (1984) states that (p. 254) that 'Some discrepancies will be seen for large deformations of long shells ... which may be attributed to the insufficient number of unknown parameters a_{mn} retained in the calculation'. The large deflection cases correspond exactly to the lower wave numbers $s = 8$ and $s = 9$. Thus given the excellent agreement with six modes for the higher wave-number cases we expect improved results with more modes for the lower wave numbers. It must also be remembered that these results are taken at the minimum load. From AUTO this minimum is found accurately (using the limit point detection facility) whereas it has to be estimated both experimentally and numerically in Yamaki (1984). This is certainly another factor in the observed discrepancies.

Our results compare favourably with the asymptotic results of Hunt & Lucena Neto (1993) who used a 16-mode approximation of fully periodic modes, together with an argument based on the Maxwell critical load, to distinguish a localized minimum. In particular we seem to capture the minimum and maximum displacement much better. This is not surprising since for the cross-symmetric solutions the maximum displacement occurs away from the mid-length of the cylinder. Note that Hunt & Lucena Neto also comment that more modes were required for lower wave numbers.

Our findings so far are preliminary and a more complete analysis including symmetric buckling patterns, and an investigation of the Maxwell load hypothesis, will form the subject of future work. We also remark, based on preliminary unreported computations and on previous experience with simpler Hamiltonian systems (Devaney 1976; Champneys & Toland 1993; Hunt *et al.* 1989) that for each mode number, s, the existence of one localized solution implies infinitely many other localized solutions. These are essentially multiple copies of the symmetric and anti-symmetric solutions separated by finite axial distances. The investigation of these multi-modal solutions is also left to future work.

One advantage of our approach is that fewer modes are required to capture the localized buckling than was used in Yamaki (1984). For $s = 10$ and $s = 11$ our six-mode approximation ($M = 6$) is as accurate as his 20-mode approximation. Another advantage of the numerical procedures used here as opposed to a finite element analysis (see, for example, Wohlever & Healey 1995), is that our methods are well suited to exploring multiplicities of solution and understanding the structure not just from the point of view of symmetries, but also from the inherent multiplicities associated with homoclinic bifurcations (see Hunt *et al.* (1997) for a comparison with finite elements in a much simpler problem).

The work in this paper lends weight to the description of the localized buckling of long thin axially compressed cylinders as a homoclinic phenomenon. We have obtained excellent agreement with experimental work on the longest elastic cylinder for which detailed experimental results could be found, with only a few circumferential modes in the numerical approximation. The localization occurs naturally as a solution to the von Kármán–Donnell equations, independently of any imperfection in the cylinder, and demonstrates that the corresponding asymptotic boundary conditions are natural boundary conditions for long cylinders.

References

Beyn, W.-J. 1990 The numerical computation of connecting orbits in dynamical systems. *IMA J. Numer. Analys.* **9**, 379–405.

Champneys, A. R. & Toland, J. F 1993 Bifurcation of a plethora of multi-modal homoclinic orbits fo autonomous Hamiltonian sytems. *Nonlinearity* **6**, 665–772.

Devaney, R. L. 1976 Homoclinic orbits in Hamiltonian systems. *J. Differ. Equat.* **21**, 431–438.

Doedel, E. & Kernevez, J. P. 1986 AUTO: Software for continuation problems in ordinary differential equations with applications. California Institute of Technology Applied Mathematics Technical Report.

Donnell, L. H. 1934 A new theory for buckling of thin cylinders under axial compression and bending. *Trans. ASME Aero. Engng* **56**, 795–806.

Donnell, L. H. & Wan, C. C. 1950 Effect of imperfections on buckling of thin cylinders and columns under axial compression. *J. Appl. Mech.* **49**, 73–83.

Friedman, M. J. & Doedel, E. J. 1994 Numerical computational of invariant manifolds connecting fixed points. *SIAM J. Numer. Analys.* **28**, 789—808.

Golubitsky, M., Marsden, J. & Schaeffer, D. 1984 Bifurcation problems with hidden symmetries. In *Partial differential equations and dynamical systems* (ed. W. Fitzgibbon), pp. 181–210. Boston, MA: Pitman.

Gottlieb, D & Orszag, S. A. 1977 *Numerical analysis of spectral methods: theory and applications.* Philadelphia, PA: SIAM.

Hagstrom, T. M. & Keller, H. B. 1987 Asymptotic boundary conditions and numerical methods for nonlinear elliptic problems on unbounded domains. *Math. Comp.* **48**, 449–470.

Hoff, N., Madsen, W. A. & Mayers, J. 1966 Post-buckling equilibrium of axially compressed circular cylindrical shells. *AIAA Jl* **4**, 126–133.

Hunt, G. W. 1986 Hidden (a)symmetries of elastic and plastic bifurcation. *Appl. Mech. Rev.* **39**, 1165–1186.

Hunt, G. W. & Lucena Neto, E. 1991 Localized buckling in long axially loaded cylindrical shells. *J. Mech. Phys. Solids* **39**, 881–894.

Hunt, G. W. & Lucena Neto, E. 1993 Maxwell critical loads for axially loaded cylindrical shells. *Trans. ASME* **60**, 702–706.

Hunt, G. W., Bolt, H. M. & Thompson, J. M. T. 1989 Structural localisation phenomena and the dynamical phase-space analogy. *Proc. R. Soc. Lond.* A **425**, 245–267.

Hunt, G. W. Lawther, R. & Providência e Costa, P. 1997 Finite element modelling of spatially chaotic structures. *Int. J. Numer. Meth. Engng.* **40**, 2237–2256.

Hunt, G. W., Williams, K. A J. & Cowell, R. G. 1986 Hidden symmetry concepts in the elastic buckling of axially loaded cylinders. *Int. J. Solids Structures* **22**, 1501–1515.

Kirchgässner, K. 1982 Wave solutions of reversible systems and applications. *J. Differ. Equat.* **45**, 113–127.

Koiter, W. T. 1945 On the stability of elastic equilibrium. Ph.D. thesis, University of Delft. (Engl. Transl. Tech. Rep. AFFDL-TR-70-25 Air Force Flight Dyn. Lab. 1970.)

Mielke, A. 1991 *Hamiltonian and Lagrangian flows on center manifolds: with applications to elliptic variational problems.* Springer Lecture Notes in Mathematics, vol. 1489. Berlin: Springer.

Sandstede, B. 1997 Convergence estimates for the numerical approximation of homoclinic solutions. *IMA J. Numer. Analysis* **17**, 437–462.

Schecter, S. 1993 Numerical computation of saddle–node homoclinic bifurcation points. *SIAM J. Numer. Analysis* **30**, 1155–1178.

Wohlever, J. C. & Healey, T. J. 1995 A group theoretic approach to the global-bifurcation analysis of an axially compressed cylindrical-shell. *Comp. Meth. Appl. Mech. Engng* **122**, 315–349.

Yamaki, N. 1984 *Elastic stability of circular cylindrical shells.* Applied Mathematics and Mechanics Series, vol. 27. New York: Elsevier.

Yoshimura, Y. 1930 On the mechanism of buckling of a circular clindrical shell under axial compression. NACA Technical Memorandum.